Applied Engineering
2023; 7(2): 37-46
http://www.sciencepublishinggroup.com/j/ae
doi: 10.11648/j.ae.20230702.12
ISSN: 2994-7456 (Online)

Development of a New Aerodynamic Method for the Mechanical Characterization of a Horizontal Axis Wind Turbine

Choupo Yuego[1, *], Maxwell Tientcheu Nsiewe[1, 2], Balbine Matuam Tamdem[1], Nicolas Gnepie-Takam[1], Alexis Kuitche[1]

[1]Laboratory of Energetics and Applied Thermics, High National School of Agro-Industrial Sciences, University of Ngaoundéré, Ngaoundéré, Cameroon

[2]School of Chemical Engineering and Mineral Industries, University of Ngaoundéré, Ngaoundéré, Cameroon

Email address:

chouposimone@gmail.com (Choupo Yuego), maxwelltientcheunsiewe@gmail.com (Maxwell Tientcheu Nsiewe)

[*]Corresponding author

To cite this article:

Choupo Yuego, Maxwell Tientcheu Nsiewe, Balbine Matuam Tamdem, Nicolas Gnepie-Takam, Alexis Kuitche. Development of a New Aerodynamic Method for the Mechanical Characterization of a Horizontal Axis Wind Turbine. *Applied Engineering*. Vol. 7, No. 2, 2023, pp. 37-46. doi: 10.11648/j.ae.20230702.12

Received: October 14, 2023; **Accepted**: October 31, 2023; **Published**: November 11, 2023

Abstract: The aim of this work is to propose a new method for calculating the aerodynamic forces of wind turbine blades and the power developed by them. To this end, the blade element momentum, prescribed wake and free wake methods were compared for speed ranges from 5 to 20m/s. The two-bladed NREL PHASE IV wind turbine with profile S 809 was used as the physical model, with the polars extrapolated to 90° using the Viterna method and then extended from -180 to 180° using flat theory. The largest error in power output was 47% at 5 m/s using PVM, the second largest was 16% at 10 m/s using BEM, and the third largest was 13% at 10 m/s using FVM. In or-der to reduce the percentage error of the PVM, the phenomen of vortex core growth has been in-tegrated into this method. The error at 5m/s was reduced from 47% to 8.29%, and the maximum error of the modified method was 9.19% observed at 18m/s. The new method was then compared to the Reynolds-averaged Navier-Stokes equation from the literature for the same velocity range. The maximum error observed was 8% at 10m/s for the RANS and 9.19% at 18 m/s for the new method.

Keywords: Aerodynamic Modeling, Horizontal Axis Wind Turbine, BEM, PVM, FVM

1. Introduction

Aerodynamic modelling techniques for wind turbines enable us to take into ac-count the various stresses to which the machine is subjected. They are also used in the design of the machine. A numerical method is said to be efficient if it has a low com-putation time and a low relative error compared with the experimental method; it is therefore important to find a compromise between simulation time and this error [1]. The major challenge of aerodynamic modeling is to successfully estimate the velocity fields and the angle of incidence. Indeed, knowledge of the various aerodynamic forces depends on these two parameters, which in turn depend on the speeds induced by the wake downstream of the wind turbine [2]. Each variation in the wake structure is accompanied by a variation in the induced velocities, followed by a variation in the relative velocity, the local angle of incidence and, consequently, the aerodynamic load on the rotor [3]. Hence the importance of taking the actual wake structure into ac-count.

Several aerodynamic modeling methods are available in the literature. The Blade Element Method (BEM), widely used for modeling the forces provided by a ro-tor [1, 4-6]. It has been modified to take into account stall attack angles (the polars have been extrapolated to 90° using Viterna's method), blade root losses [7-10]. And the vertical wind gradient upstream of the rotor [11]. Because it relies on several correc-tion factors, BEM is not very accurate. In addition, it assumes that the wake down-stream of the rotor is like a cylindrical tube. In fact, an experiment conducted by the NREL laboratory on a wind

turbine equipped with a blade tip smoke generator shows that the wake downstream of a rotor has a helical shape.

The prescribed wake method (PVM) used by Burton, D and al. for wind turbines assumes that the wake is known on the basis of approximate calculations [12]. The wake is modeled by a set of concentric circles, helices or rigid vortex segments [13-15]. Work carried out on a NACA 4412 blade profile proposed two prescribed wake shapes [16]: the first, modeled by helicoids, and the second by concentric circles: the difference between numerical and experimental is greater (of the order of 23%) for the first wake shape versus around 15% for the second shape. The experiment conducted by the NREL la-boratory shows that the wake radius increases towards infinity downstream of the flow. In its basic formulation, PVM does not take this phenomenon into account.

The free wake method (FVM), on the other hand, uses a Lagrangian description of the flow by placing markers along the helicoids [2, 17, 18]; the wake is built up over time by vortex segments located between two markers. The velocities induced at the rotor plane by each segment making up the wake are determined by Biot and Savart's law [2]. This law admits a singularity for vortex segments close to the control point. To deal with the singularity, the β-Vatista method [19] is recommended for n=2 and for parameter β varying between 1.47 and 1.72. In addition to a wake consisting of vortex segments free to move, the literature proposes a wake consisting of concentric circles free to move and deform relative to each other [16, 20]. The work of Xu, B and al. leads to the conclusion that, the results provided when the wake is modeled by circles are as accurate as those thus the wake is constituted progressively by vortex segments [20]. What's more, it saves computation time.

In this work, we propose a stationary aerodynamic method based on the pre-scribed wake of concentric circles. Taking into account the vortex at the blade root and the increase in the vortex core. In order to validate the method, it is compared with the aforementioned methods. Then compared with the Reynolds averaging method using the Navier-Stokes equations (RANS).

2. Material and Methods

2.1. Material

The rotor is a NREL Phase IV two-bladed rotor with the S809 blade profile [21]. The table I shows the rotor's geometric characteristics.

Table 1. *Rotor's geometric characteristics.*

r_{da}(m)	r_{fa}(m)	N	Θ[°]	Ω[tr/mn]	D[m]	Rotor blade profile
1,2573	4,903	2	3	71,63	10	S809 twisted

The chord has a value of 0.7366 m at the root and 0.38m at the tip. The twist an-gle is 21.8° at root and -1.775° at blade tip.

2.2. Aerodynamic Method

In analytical or semi-analytical aerodynamic methods, the wind rotor is divided into several slices, denoted "dr", and the study is carried out slice by slice. The slices are assumed to be aerodynamically independent of each other [1, 12]. On a blade element, the expressions for axial force and moment are given by equations 1 and 2.

$$dT = \rho N(C_L \cos\phi + C_D \sin\phi)cdr\, V_0^2(1-a)^2/(2\,(\sin\phi)^2) \quad (1)$$

$$dM = \rho V_0 \Omega \mathrm{N} c(1-a)(1+a')(C_L \sin\phi - C_D \cos\phi)r^2 dr/(2\sin\phi\, cos\phi) \quad (2)$$

Where ρ is density; a is the axial induction coefficient; a' the tangential induction coefficient; c_i the elementary chord; ϕ the flow angle (rad); C_D the coefficient of drag; and C_L the coefficient of lift; V_0 wind speed;

Relative velocity (W), flow angle (ϕ) and angle of attack (α) are given by Equations 3, 4 and 5 respectively. Equation 6 gives us the elementary power.

$$W = \sqrt{((1-a)V_0)^2 - ((1+a')\Omega r)^2} \quad (3)$$

$$\tan(\phi) = (1-a)V_0/(1+a')\Omega r \quad (4)$$

$$\alpha = \phi - \beta \quad (5)$$

$$dP = (1/4)\rho c(C_L \sin\phi - C_D \cos\phi)\, NW^2 \Omega r dr \quad (6)$$

According to Equations 1, 2, 3, 6, the estimation of the velocity and elementary force fields depends directly on the axial and tangential induction coefficients. Which, in turn, depend on the shape of the wake downstream of the wind turbine. For a fixed wing in a flow, the effects induced by the wake fade rapidly after a few chords. For a rotating wind turbine blade, on the other hand, this limited influence of the wake is not observed. It is therefore important to take this phenomenon into account in order to estimate the optimum aerodynamic load. The wake downstream of a wind turbine blade is dominated by two marginal vortices: one emanating from the blade root, the other from the blade tip [2]. There are several methods for determining induced velocities.

2.2.1. Glauert's Method

Known as the Blade-Element-Momentum method (BEM), the rotor is treated here as an active disc that extracts the kinetic energy available in the wind. This is equivalent to assuming an infinite number of blades [1]. This assumption is corrected by the Prandlt factor. The presence of the disc creates a pressure discontinuity. By applying Bernouillie's theorem upstream and downstream of the rotor, we obtain the expressions for axial force and moment (Equations 7 and 8) [4].

$$dF_a = 4\pi r \rho V_0^2 a(1-a)dr \quad (7)$$

$$dM = 4\pi r^3 \rho V_0 \Omega(1-a)a' dr \quad (8)$$

Equating Equations 1 and 7, and Equations 2 and 8, we

deduce the expressions for the axial and tangential coefficients given by Equations 9 and 10. Where F (Equation 11) is the Prandlt factor.

$$a = 1/(1 + (4Fsin\phi^2/\gamma C_{fX})) \quad (9)$$

$$a' = (1/((4Fsin\phi cos\phi/\gamma C_{fY}) - 1 \quad (10)$$

With

$$F = (2/\pi)arcos\left[e^{(N(R-r)/2r\sin\phi)}\right] \quad (11)$$

The expressions for elementary power and moment are modified according to Equations 12 and 13 [12].

$$dP = (1/4)\rho c(C_L \sin\phi - C_D \cos\phi)\, FNW^2 V_r dr \quad (12)$$

$$dM = (\rho V_0 \Omega NF/2\sin\phi)((1-a)(1+a')/cos\phi)(C_L \sin\phi - C_D \cos\phi)cr^2 dr \quad (13)$$

The wake downstream of the wind turbine in this method is considered to be a cylindrical sheet of radius R (Figure 1). The calculation flowchart is shown in Figure 2.

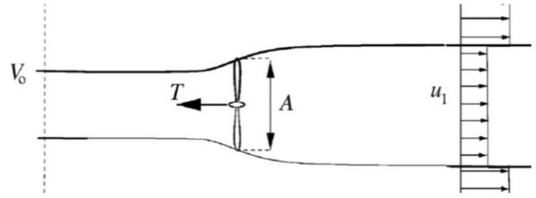

Figure 1. *Wake shape downstream of the wind turbine for BEM [12].*

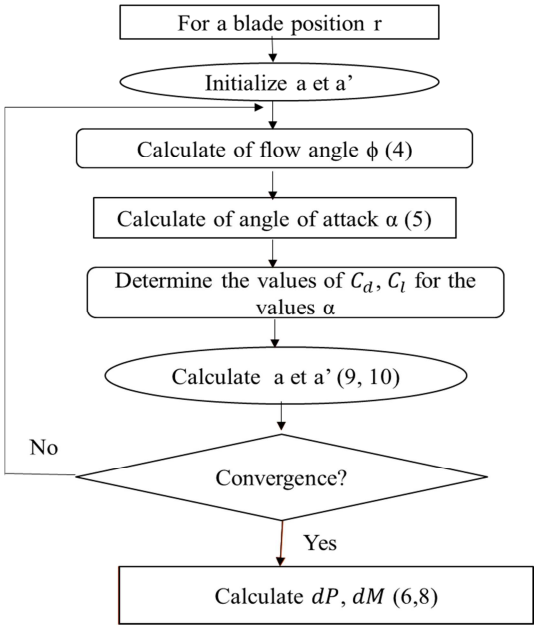

Figure 2. *BEM calculation algorithm [1, 4].*

2.2.2. Prescribed Wake Method (PVM)

This method consists in considering the wake downstream of the wind turbine, based on tests or available data (in our case, we used data from the BEM). The wake is considered as a set of concentric circles of radius R, with constant pitch P, and vortici-ty dΓ emanating from the blade tip; and swirl segments emanating from the blade root (Figure 3) [1, 15, 16].

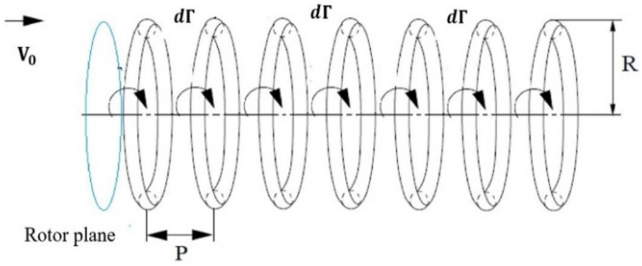

Figure 3. *Wake shape downstream of the wind turbine for PVM [16].*

$$d\Gamma = 4\pi a(1-a)V_0^2/\Omega(1+a') \quad (14)$$

$$p = 2\pi(1-a)V_0/\Omega \quad (15)$$

$$v = aV_0 \quad (16)$$

Induced velocities at the rotor plane are determined from the first- and second-order elliptic integrals K and E according to Equations 17 and 18 for concentric circles. For swirl segment there are determined from the Biot and Savart law.

$$V_r(r,z) = v = \left(-\Gamma/2\pi\sqrt{z^2+(r+R)^2}\right)\left(K(s) + (R^2 - r^2 - z^2/z^2 + (R-r)^2)E(s)\right) \quad (17)$$

$$V_z(r,z) = u = \left(-\Gamma/2\pi\sqrt{z^2+(r+R)^2}\right)\left(K(s) - (R^2 + r^2 + z^2/z^2 + (R-r)^2)E(s)\right) \quad (18)$$

Where s is the argument given by Equation 19, and the relative speed in this case is given by Equation 20.

$$s = \sqrt{4rR/(z^2+(r+1)^2)} \quad (19)$$

$$W = \sqrt{(V_0 - v)^2 - (U_0 + u)^2} \quad (20)$$

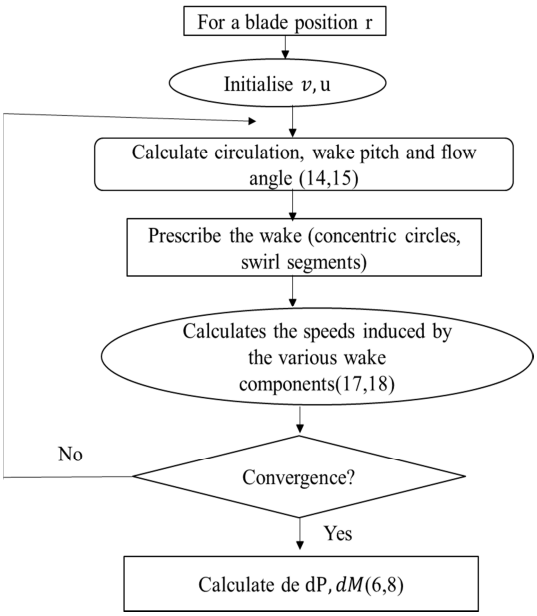

Figure 4. *PVM calculation algorithm [1, 17].*

The shape of the wake is shown in Figure 4, and the calculation flowchart is given in Figure 5.

The induced velocities are initialized using Glauert's method, and the corresponding initial wake shape is generated. Subsequently, the wake-induced velocities at the rotor plane are calculated using the vortex method (Equations 17, 18). These differ from the initialized speeds. An iterative procedure is used until the induced velocity converges.

2.2.3. The Free Wake Method (VFM)

This method involves a Langrangian study of the flow. Langrangian markers are placed along the helicoids making up the wake (Figure 5) [2], The wake is thus made up of a set of vortex segments located between two markers.

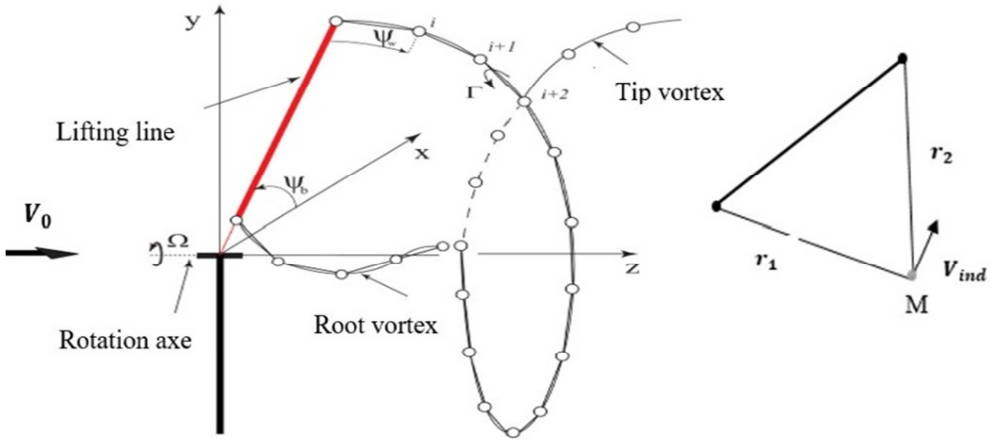

Figure 5. *Progressive wake construction using FVM [2].*

The blade is modeled as a lifting line at the origin of the lift It is subdivided into several segments of vortex intensity Γ_i given by the Koutta-Joukowski law (Equation 21) [20]. The velocity induced at point M of the rotor plane by each vortex segment constituting the wake is given by Biot and Savart's formula (Equation 22) [17].

$$\Gamma_i = (1/2)c_i C_l W_i \tag{21}$$

$$\vec{V}_{ind} = (C_v\Gamma_v/4\pi) \times \left((|\vec{r}_1| + |\vec{r}_2|).(\vec{r}_1 \wedge \vec{r}_2)/|\vec{r}_1|.|\vec{r}_2|.(|\vec{r}_1|.|\vec{r}_2| + \vec{r}_1.\vec{r}_{2)}\right) \tag{22}$$

Where

$$C_v = (L|\vec{r}_1|)^2 - \left(\vec{r}_1.\vec{L}\right)^2/L^2\left(r_c^{2n} + \left((L|\vec{r}_1|)^2 - \left(\vec{r}_1.\vec{L}\right)^2\right)/L^2\right)^{2n}\Big)^{1/n} \tag{23}$$

The C_v term in Equation 22 removes the singularity present in Biot and Savart's law for a vortex segment close to the control point. Taking into account the radius of curvature r_c of the segment. In our study, we have taken n=2. The wake is built up over time by solving the marker equation (Equation 24) [2]. The growth of the vortex core is taken into account by Equation 25 as proposed by [22].

$$\frac{\partial\vec{r}}{\partial\psi_w} + \frac{\partial\vec{r}}{\partial\psi_b} = (1/\Omega)\left(\vec{V}_0 + \sum_{j=1}^{Ns}\vec{V}_{ind}(\vec{r},t)\right) \tag{24}$$

$$r_c(\psi_w) = \sqrt{r_0^2 + 4\alpha_s\delta_s\nu\psi_w/\Omega} \tag{25}$$

The parameter δ_s quantifies the rate of diffusion of the filament from the tip of the blade. It is a function of the Reynolds number:

$$\delta_s = 1 + a_1 Re_\nu \tag{26}$$

With $Re_\nu = \Gamma/\nu$; $\delta_s$is the oder of 10^4.

The flow chart of the method is given in Figure 6.

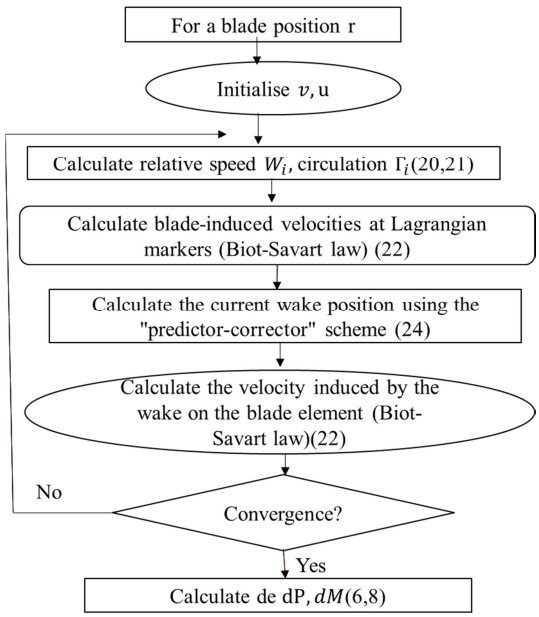

Figure 6. *FVM calculation algorithm [1, 17, 19].*

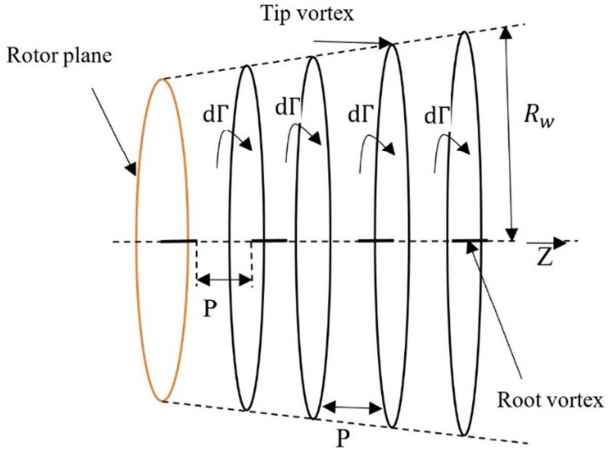

Figure 7. *Wake shape downstream of the wind turbine.*

BEM has the advantage of converging rapidly. However, it is not a very accurate method. This is because it is based on a set of corrective parameters. In addition, the wake downstream of the wind turbine is considered to be an infinitely long cylinder of radius R. VFM, on the other hand, takes into account the actual wake structure downstream of the wind turbine. However, it takes a sufficiently long time for the system to stabilize. After that, the elementary power value varies very little (of the order of 1/1000). PVM therefore represents a good balance between computation time and accuracy [20]. However, in its basic formulation, it has some shortcomings: the phenomenon of vortex core growth is not taken into account. The remainder of this article takes this phenomenon into account (Figure 7): The notion of vortex core evolution is of crucial importance for wind farms; in a farm, several turbines may operate in the shadow of the front-line turbines. As a result, the wind turbines inside the farm receive wind that is not only reduced in speed, but also turbulent. This greatly reduces the farm's efficiency. Several models have been developed to consider this phenomenon. However, Larsen's model (2009) [23] is the most widely used and has proven its worth [24-26]. The expression of the evolutionary radius is given by Equation 27.

$$R_w(z) = (105C_1^2/2\pi)^{1/5}\left(C_T\Omega(z+z_0)\right)^{1/3} \quad (27)$$

With

$$C1 = (kD_0/2)^{5/2}(105/2\pi)^{-1/2}(C_T\Omega z_0)^{-5/6} \quad (28)$$

Where: $z_0 = 9{,}6D_0/\left(\left(2R_{9,6}/kD_0\right)^3 - 1\right)$; $k = \sqrt{(m+1)/2}$; $m = 1/\sqrt{1-C_T}$, and

$$R_{9,6} = a_1 e^{(a_2C_T^2 + a_3C_T + a_4)}(b_1I_a + 1)D_0$$

Where I_a is the turbulence intensity; values a_1, a_2, a_3, a_4, b_1 are contained in Table 2.

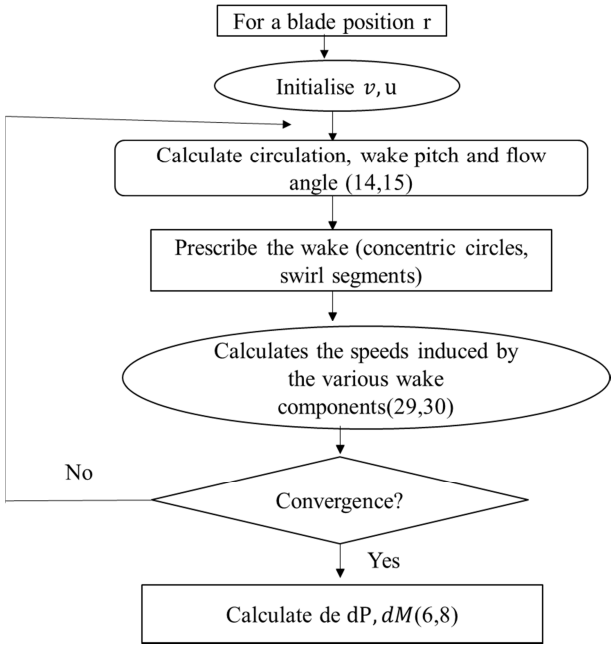

Figure 8. *Calculation algorithm.*

Table 2. *Coefficients of Larsen [23].*

Coefficients	a_1	a_2	a_3	a_4	b_1
Values	0.43544986	0.797853685	-0.124807893	0.136821858	15.6298

Equations 29 and 30 are the new expressions of the velocities induced by concentrics circles on the rotor plane.

$$V_r(r,z) = v = \left(-\Gamma/2\pi\sqrt{z^2+(r+R_w)^2}\right)\left(K(s) + (R_w^2 - r^2 - z^2/z^2 + (R_w - r)^2)E(s)\right) \quad (29)$$

$$V_z(r,z) = u = \left(-\Gamma/2\pi\sqrt{z^2+(r+R)^2}\right)\left(K(s) - (R_w^2 + r^2 + z^2/z^2 + (R_w - r)^2)E(s)\right) \quad (30)$$

The calculation flowchart is shown in Figure 8.

The available polars were extrapolated to 90° using the Viterna model [27]. These were then extended from -180° to 180° using flat theory. Induced velocities from BEM are used to initialize PVM, FVM. The flow was simulated for a velocity range from 5 to 20 m/s.

3. Results

Figure Figures 9 and 10 show the evolution of power and power coefficient for different speeds.

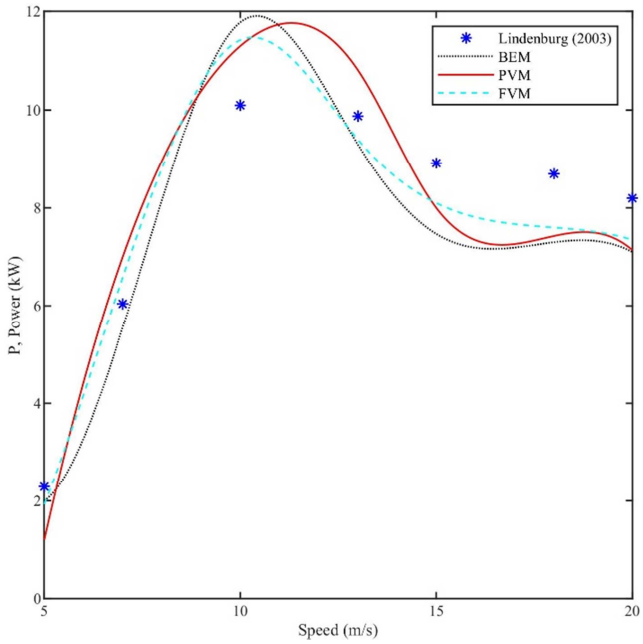

Figure 9. *Evolution of power for different speed.*

At first glance, we can see that the power curves provided by the different methods have the same appearance as those obtained from the experiment. In more detail, the power increases with a steep slope up to 10 m/s and then oscillates between 8Kw and 10Kw. The fact that the power no longer increases is due to aerodynamic braking [1].

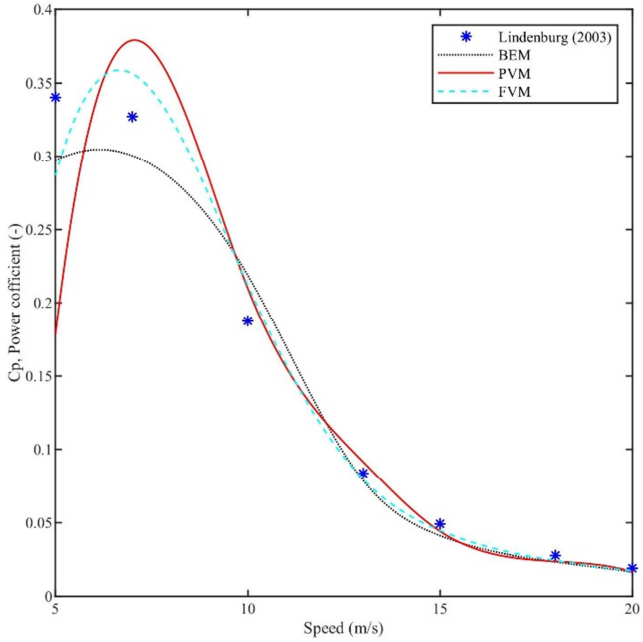

Figure 10. *Evolution of coefficient power for different speed.*

The start-up speed of this wind turbine is around 4 m/s. Between this speed and around 5 m/s, we are dealing with natural convection, which would justify the huge error in the PVM at 5 m/s. Between 5 and 10 m/s, which is the turbine's rated speed, power increases and reaches its rated power of 10 kW. In fact, power increases with the cube of the speed. After this speed, the braking devices are activated to keep the turbine's rotation speed constant; this enables the rated power (10 kW) to be maintained regardless of the incoming wind speed. However, speed variation creates vortices in the flow and causes power drops as seen at 15m/s, 18m/s and 20m/s.

Figure 11 shows in diagram form the relative errors of the power supplied by the different methods compared with the experimental one.

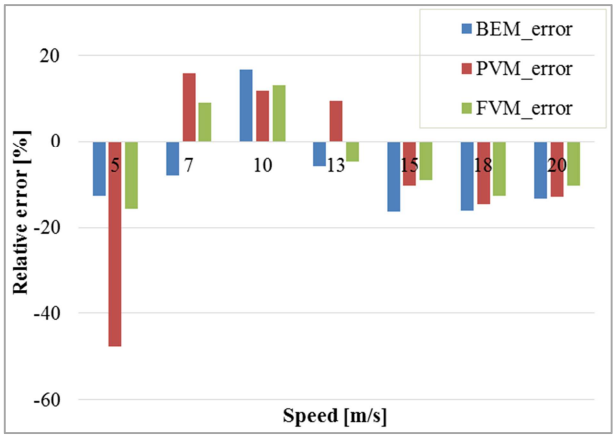

Figure 11. *Relative error for different speed.*

The PVM underestimates the natural convection phenomenon expressed at 5 m/s with an error of 47%, while for the increasing slope, between 7 and 10 m/s, it overestimates with errors of 15.89 and 11.88% respectively. This one (PVM) doesn't translate the power drops between 15 and 20m/s very well either. However, the smallest errors are observed at 10 and 13m/s. And the method provides the best estimate of rated power at 10m/s.

The FVM follows in the footsteps of the BEM, better reflecting the natural convection phenomenon, but predicts the nominal power value with an error of 13.069%. Power drops at 15 and 20 m/s benefit from errors of -9.19% and -10.36% respectively; these are the smallest errors recorded for these speeds.

Of the three methods, we can conclude that:

1) BEM seems adequate for low wind speeds, with the smallest errors recorded at 5 and 7 m/s and the largest at 15m/s, although 13m/s is the exception. The accuracy of the BEM for low wind speeds and the divergence around the nominal speed are also observed in the work of [28], and those produced by the commercial software XFOIL. However, for high velocities, [28] produce results with better accuracy than the present work, due to the fact that in their simulation, the polars were not extrapolated from -180 to 180.
2) PVM seems more appropriate for medium wind speeds, with the smallest error recorded at 13m/s and the two largest at 7 and 18m/s. The work of [16] using the same method leads to the same conclusion.
3) The FVM is suitable for high wind speeds; in fact, of the three methods, it provides the lowest errors for speeds of 13, 15, 18 and 20 m/s.

Generally speaking, PVM produces the greatest error of the

three methods, 47% at 5 m/s, and FVM the smallest (4.85%) at 13 m/s. The phenomenon of vortex growth was integrating into PVM in order to improve its accuracy and make it more competitive. Indeed [12], in establishing Eq. 14, have cancelled out vortex growth.

Figure 12 shows the power curve produced by the proposed method (called NEW METHOD in the various figures) compared with that produced by previous methods.

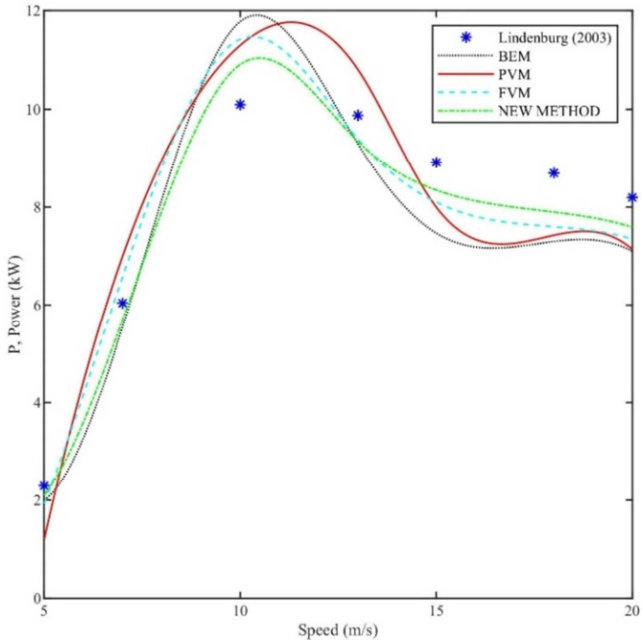

Figure 12. *Evolution of power for different speed.*

We can safely say that it is closer to the experimental curve than PVM. Indeed, its shape is closer to the experimental one. Figure 13 shows the power coefficient for all the methods used.

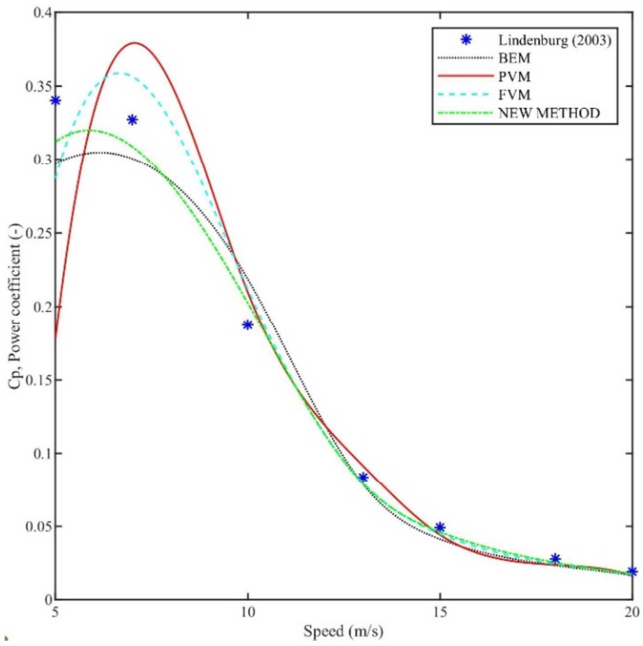

Figure 13. *Evolution of coefficient power for different speed.*

Figure 14 shows the relative errors between the different methods and the experimental model.

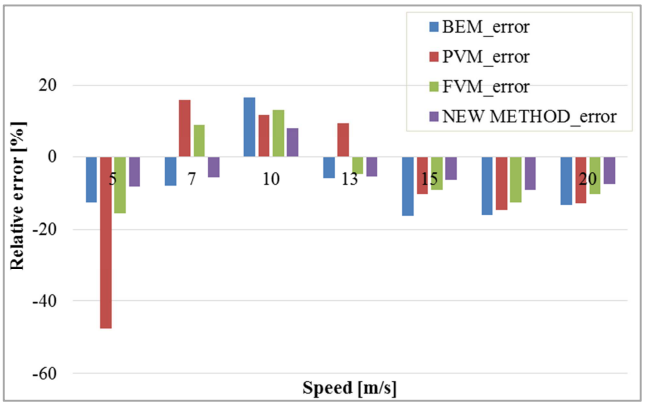

Figure 14. *Relative error for different speed.*

The proposed method better reflects the natural convection phenomenon, with an error of -8.29% compared with 47% produced by PVM. This error is smallest at 5m/s for the different methods compared. At 10m/s, the present work predicts a power of 10.91Kw, i.e. an error of 8.01%. It overtakes PVM, which had the best prediction at this speed let be 11.88% versus 16.63% and 13.06% for BEM and FVM respectively. In terms of power loss, it has an error of -6.39 and -7.49% respectively for speeds of 15 and 20m/s, compared with -9.18 and -14.02%, -10.31 and-14.63%, -16.25 and 16.09% for FVM, PVM and BEM respectively. The errors recorded at speed points 15 and 20m/s by the present study are therefore the lowest errors recorded for these two speeds.

The maximum relative error for the present study is 9% observed at 18m/s. This is lower than the maximum relative errors produced by the other methods, which are 47%, observed at 5m/s by the PVM, the second is 16% observed at 10m/s by the BEM, and the third is 13% observed at 10m/s by the FVM. Looking at the trend in errors produced by the present study for each speed, it can be said that it is adequate whatever the speed range (small, medium and large). In fact, it has a low average error whatever the incoming wind speed. Finally, by including the phenomenon of vortex accretion, the maximum relative error of the PVM was reduced from 47% at 5m/s to 9% at 18m/s.

For the sake of validation, we made a comparison with the work of Derakhshan, S and al. [29] who worked on the same rotor using Reynolds averaging by Navier-Stokes equations (RANS) and Ansys-CFD as software. Figure 15 shows the evolution of the power supplied by both NEW and the numerical method called NUM. The dark blue asterisks represent the experimental data, the green solid lines NEW and the magenta NUM. It can be seen that both power curves have the same shape. The nominal power supplied by NUM is 10.54 kW, compared with 10.91 kW supplied by NEW, which is closer to the experimental value of around 10 kW.

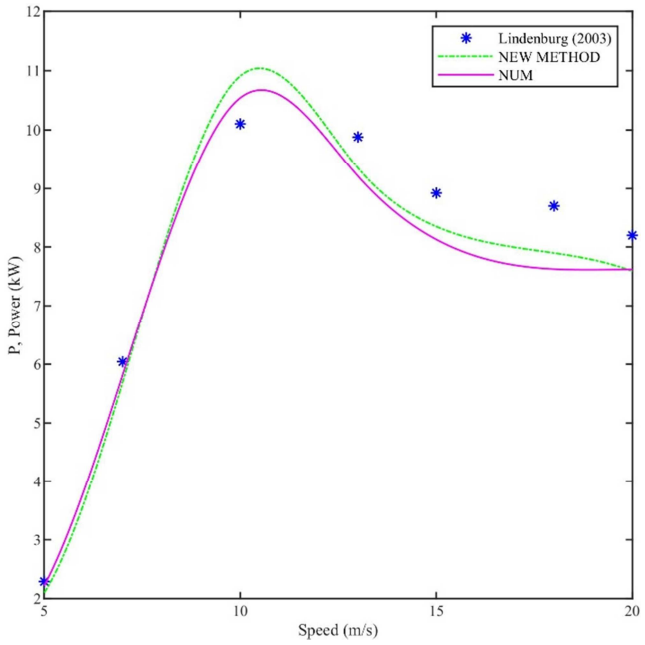

Figure 15. *Evolution of power for different speed.*

Figure 16 shows the relative error diagram of the power supplied by the two methods compared with the experimental one. The latter shows that NUM benefits from a minimum error for velocities ranging from 5 to 10m/s, but for higher velocities it provides higher errors; this shortcoming of NUM has already been noted by Chechouri, A and al. [30]. For high speeds, however, the proposed method can be relied on with confidence. Indeed for the speed range from 13 to 20m/s this method provides a relatively low error compared to NUM. From this figure we can also see that the largest error provided is 8.89% for NUM and 9.29% for NEW. The difference between the two maximum errors is small (less than 1%), which allows us to state that the proposed method is as efficient as the Reynolds averaging method using the Navier-Stokes equations (RANS).

Figure 16. *Evolution of relative error for different speed.*

Figure 17 shows the torque of the aerodynamic forces involved. Generally speaking, whatever the incoming wind speed, it can be seen that the proposed method is closer to the experimental one than the others. In fact, it better translates the torque provided at 5 m/s, better captures the maximum moment at 10m/s and at 18m/s it also has the best estimate. This supports the conclusion that this method can be used whatever the speed range.

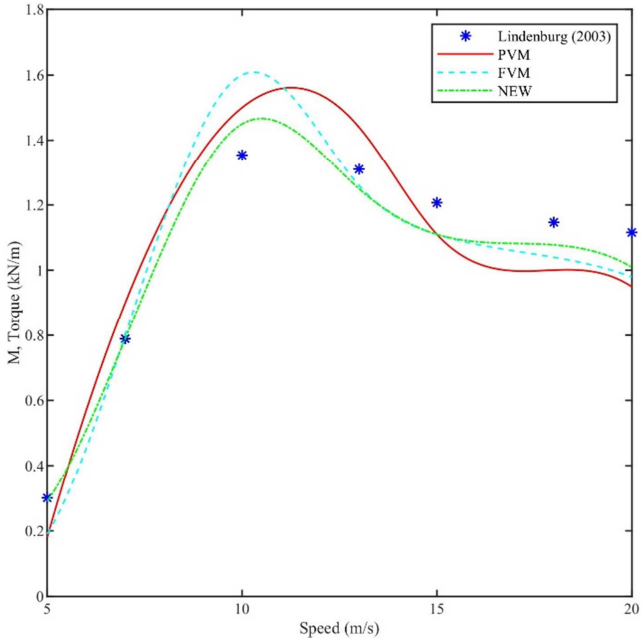

Figure 17. *Evolution of torque for different speed.*

For a speed of 10m/s, Figure 18 shows the evolution of R_w with depth z over a distance of 4R. It can be seen that R_w reaches a value of around 5.5m at a depth of 10m and a value of 5.7m at 20m. In more detail, it can be seen that R_w increases with depth z; between 0 and 2m, the growth slope is steep, but decreases with depth.

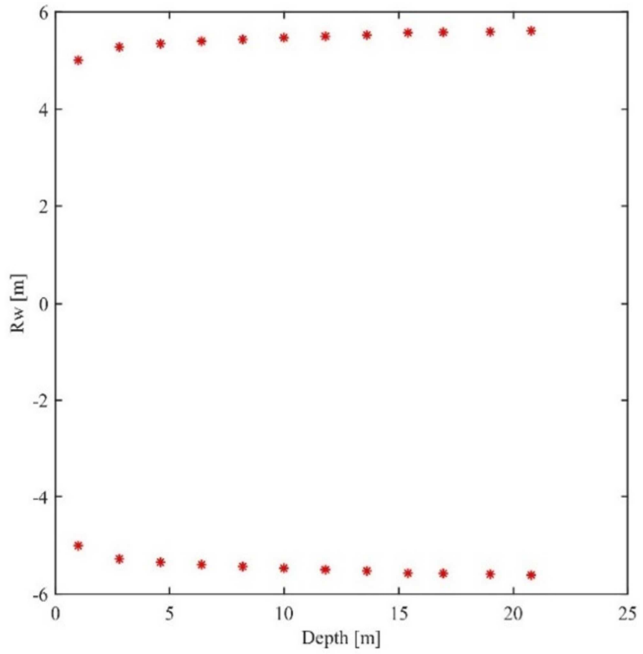

Figure 18. *Evolution of R_w as a function of depth.*

The influence of an increase in radius R_w on the power

supplied was evaluated through two actions: an increase and a decrease in R_w:

1) Increasing R_w by 0.01 and 0.05m reduces power output from 10.85 kW to 8.92 and 7.18 respectively.
2) Decreasing the radius by 0.01 and 0.05m increases the power from 10.85 kW to 13.62 and 46.93kW respectively.

A slight increase in R_w resulted in an underestimation of power of the order of 17% and 33%. On the other hand, a slight decrease, which in other words reduces or even cancels its influence, causes an overestimation of the order of 25% and over 100%. This would explain the tendency of the prescribed wake method (PVM) to overestimate output power. Indeed, in the relative error diagram (Figure 14), it is found three times above zero, compared with once for the proposed method (NEW). These two actions clearly demonstrate the importance of taking into account core growth in the wake structure downstream of the wind turbine. In concrete terms, failure to take into account vortex buildup leads to an overestimation of the turbine's power output, and could therefore distort the expectations of a lambda customer, and create problems for the promising wind energy sector.

The influence of depth z on power output was assessed by limiting the wake length to 2R, 3R, 4R, 5R and 6R, and it was found that power evolves with wake length. However, for a value of z beyond 4R, the influence of the wake becomes less pronounced. Indeed, for a depth of x=5R and x=6R the power supplied is 10.87kW and 10.91kW. An increase of 0.007 and 0.06 respectively. These results are in line with the limit of the influence of the 4R wake proposed by Vermeer.

4. Conclusion

In this study, a new aerodynamic method based on the prescribed wake method has been proposed: blade tip vortices are assimilated to concentric circles of evolving radius R_w; blade root vortices, for their part, are considered as a set of vortex segments. The proposed method was used to predict the power developed by a two-bladed NREL PHASE IV wind turbine for a speed range from 5 to 20m/s. The blade element method (BEM), the prescribed wake method (PVM) and the free wake method (FVM) were used on the same physical model. A comparison was made between the proposed method, BEM, PVM, FVM and RANS. The largest error observed is around 8% for CFD at 15m/s and 9% for the proposed method. This proposed model is as accurate as CFD and benefits from low computation time.

Conflicts of Interest

The authors declare that they have no conflicts of interests.

References

[1] Berlu "calcul des efforts subit par une éolienne moyenne et forte puissance», PhD thesis defended at the university of Sciences and Technologies of Lille 1, (2000), 360 pages.

[2] Chkir "Contribution à l'étude aérodynamique d'une ´éolienne par une méthode de sillage libre'', PhD thesis defended at the national school of art and profession, Paris France, (2010), 136 pages.

[3] Maalouf "Étude des phénomènes tourbillonnaires dans le sillage éolien'' PhD thesis defended at the national school of art and profession, Paris France, (2010), 149 pages.

[4] Mahri, M. S. Rouabah et S. Zid "Calcul des efforts aérodynamiques agissant sur les pales d'une petite éolienne », Revue des Energies Renouvelables Vol. 10 N°2 (2007) pp 241–256.

[5] Guang, W. Long, Z. Wei, X. Bofeng and C. Li "Large-scale wind turbine blade design and aerodynamic analysis", Chin Sci Bull, 57 (2012) pp 466–472, doi: 10.1007/ s11434-011-4856-6, doi: 10.1007/s11434-011-4856-6.

[6] Padmanabhan and R. Saravanan "Study of the Performance and Robustness of NREL and NACA Blade for Wind Turbine Applications", European Journal of Scientific Research ISSN 1450-216X Vol. 72 No. 3 (2012), pp. 440-446.

[7] Shen, R. Mikkelsen and J. N. Sørensen. "Tip Loss Corrections for Wind Turbine Computations", Wind Energy 8 (2005) pp 457-475.

[8] Clifton and D. H. Wood "Further dual purpose evolutionary optimization of small wind turbine blades", Journal of Physics: Conference Series 75 (2007) pp 012-017, doi: 10.1088/1742-6596/75/1/012017.

[9] Hassanzadeh, A. H. Hassanabad, and A. Dadvand "Aerodynamic shape optimization and analysis of small wind turbine blades employing the Viterna approach for post - stall region" Alexandria Engineering Journal 55 (2016), 2035-2043 Alexandria Engineering Journal (2016) 55, 2035–2043, doi.org/10.1016/j.aej.2016.07.008.

[10] Khchine and M. Sriti "Tip loss factor effects on aerodynamic performances of horizontal axis wind turbine", energy procedia 11 (2017) pp 136-140.

[11] Kavari, M. Tahani and M. Mirhosseini "Wind Shear Effect on Aerodynamic Performance and Energy Production of Horizontal Axis Wind Turbines with Developing Blade Element Momentum Theory", Journal of Cleaner Production 073 (2019), pp 1-22 doi: 10.1016/j.jclepro.2019.02.073.

[12] Burton, D. Sharpe, N. Jenkins E. Bossanyi "Wind Energy Handbook'' ed John Wiley and Sons, ISBN 0-471-48997-2 Library of Congress, (2001) 644 pages.

[13] Kocurek "Lifting surface performance analysis for horizontal axis wind turbines", Solar Energy Research Inst., Golden, CO (USA) (1987).

[14] Dumitrescu and V. Cardos "Wind Turbine Aerodynamic Performance by Lifting Line Method ", Int. J. Rotating Mach., vol. 4 no. 3, (1998) pp. 141–149.

[15] Currin, F. N. Coton and B. Wood "Dynamic Prescribed Vortex Wake Model for aerodyn/fast" Journal of Solar Energy Engineering vol. 130, no. 3, (2008) pp 31007.

[16] Meglagloui "contribution à l'étude d'une chaine de conversion éolienne de faible puissance à axe horizontal" PhD thesis defended at the university of Badji Mokhtar-Annaba Algeria (2018), 96 pages.

[17] Sebastian, M. A. Lackner "Development of a free vortex wake method code for offshore floating wind turbines", Renewable Energy 46 (2012) pp 269-275, doi: 10.1016/j.renene;2012.03.033.

[18] Rodriguez, J. Jaworski, J. Michopoulos "Stability of helical vortex structures shed from flexible rotors" Journal of Fluids and Structures 104 (2021), pp 1-27, doi.org/10.1016/j.jfluidstructs.2021.103279.

[19] Xu, J. Feng, T. Wang, Y. Yuan, and Z. Zhao "Application of a turbulent vortex core model in the free vortex wake scheme to predict wind turbine aerodynamics" journal of renewable and sustainable energy 10, (2018) pp 1-15.

[20] Xu, T. Wang, Y. Yuan, Z. Zhao, H. Liu "A Simplified Free Vortex Wake Model of Wind Turbines for Axial Steady Conditions", Appl. Sci. 8, (2018) pp 1-18.

[21] Lindenburg "Investigation into rotor blade aerodynamics ", ECN-C-03-025, (2003), 114 pages.

[22] Leishman, J Gordon. 2002. "Challenges in modelling the unsteady aerodynamics of wind turbines" Wind Energy: An International Journal for Progress and Applications in Wind Power Conversion Technology 5 (2 3) pp 85-132.

[23] Larsen T J, Madsen H Aa, Gunner C. Larsen G C, Hansen K S. Validation of the dynamic wake meander model for loads and power production in the Egmond aan Zee wind farm. Wind Energy, Vol. 2 (2013), pp 605-624.

[24] Göçmen, Tuhfe, Paul Van der Laan, Pierre-Elouan Réthoré, Alfredo Peña Diaz, Gunner Chr Larsen, et Søren Ott. ''Wind turbine wake models developed at the technical university of Denmark: A review''. Renewable and Sustainable Energy Reviews 60 (2016) pp 752-769.

[25] Brusca, Sebastian, Rosario Lanzafame, Fabio Famoso, Antonio Galvagno, Michele Messina, Stefano Mauro, et Mauro Prestipino. "On the wind turbine wake mathematical modelling''. Energy Procedia 148 (2018) pp 20-29.

[26] Zhan, Lu, Stefano Letizia, et Giacomo Valerio Iungo. "Optimal tuning of engineering wake models through lidar measurements''. Wind Energy Science 5 (4) (2020) pp 1601-22.

[27] Viterna, Larry A. and Janetzke, David C. (NASA Lewis Research Center); 'Theoretical andexperimental power from large horizontal-axis wind turbines'. SERI/CP-635-1340, Vol. II (1981) pp 265-280.

[28] Polat, Ozge, and Ismail H Tuncer "Aerodynamic shape optimization of wind turbine blades using a parallel genetic algorithm", Procedia engineering 61 (2013), pp 28 31, doi: 10.1016/j.proeng.2013.07.088.

[29] Derakhshan and A. Tavaziani "Study of Wind Turbine Aerodynamic Performance Using Numerical Methods", Journal of Clean Energy Technologies, Vol. 3, No. 2, (2015) pp 83-90.

[30] Chehouri, Adam, Rafic Younes, Adrian Ilinca, et Jean Perron. 2015. "Review of performance optimization techniques applied to wind turbines". Applied Energy 142: pp 36 88 doi.org/10.1016/j.apenergy.2014.12.043.